Applied Physics Letters

Low-temperature fabrication of carbon-electrode based, hole-conductor-free and mesoscopic perovskite solar cells with power conversion efficiency > 12% and storage-stability > 220 days

Cite as: Appl. Phys. Lett. **117**, 163501 (2020); https://doi.org/10.1063/5.0025442
Submitted: 15 August 2020 . Accepted: 06 October 2020 . Published Online: 19 October 2020

Tingting Shi, Siyuan Lin, Mei Fang, Deming Kong, Yongbo Yuan, Yongli Gao, Bingchu Yang, Hongwei Han, and Conghua Zhou

AIP Publishing

Applied Physics Letters ARTICLE scitation.org/journal/apl

Low-temperature fabrication of carbon-electrode based, hole-conductor-free and mesoscopic perovskite solar cells with power conversion efficiency > 12% and storage-stability > 220 days

Cite as: Appl. Phys. Lett. **117**, 163501 (2020); doi: 10.1063/5.0025442
Submitted: 15 August 2020 · Accepted: 6 October 2020 ·
Published Online: 19 October 2020

View Online Export Citation CrossMark

Tingting Shi,[1] Siyuan Lin,[1] Mei Fang,[1] Deming Kong,[1] Yongbo Yuan,[1] Yongli Gao,[1,2] Bingchu Yang,[1] Hongwei Han,[3] and Conghua Zhou[1,a)]

AFFILIATIONS

[1]Hunan Key Laboratory of Super-microstructure and Ultrafast Process, School of Physics and Electronics, Central South University, Changsha 410083, Hunan, People's Republic of China

[2]Department of Physics and Astronomy, University of Rochester, Rochester, New York 14627, USA

[3]Michael Grätzel Center for Mesoscopic Solar Cells, Wuhan National Laboratory for Optoelectronics, Huazhong University of Science and Technology, Wuhan 430074, Hubei, People's Republic of China

[a)]**Author to whom correspondence should be addressed:** chzhou@csu.edu.cn

ABSTRACT

A low-temperature fabrication routine is developed for hole-conductor-free and mesoscopic perovskite solar cells using a TiO_2 nanoparticle-binding carbon electrode as the top electrode. Vacuum treatment is adopted to help the infiltration and formation processes of the organic–inorganic hybrid perovskite crystallites. It is observed that such treatment not only condenses the mesoporous skeleton and improves film conductance of the carbon electrode but also makes the perovskite crystallites grow in the core part of the mesoporous skeleton. As such, the extraction process of photogenerated charge carriers is accelerated due to the strengthened interfacial contact between the perovskite crystallites and the skeleton. Accordingly, the photo-to-electric power conversion efficiency of the low-temperature devices is upgraded from 7.38 (±1.40)% to 10.17 (±0.86)% (optimized at 12.29%, AM 1.5 G, 100 mW/cm^2). In addition, prolonged stability is observed. Due to the condensed device structure, storage stability of 225 days has been achieved in ambient air (with relative humidity of about 40–60%), even without encapsulation. The proposed strategy is helpful in further reducing the production cost.

Perovskite solar cells (PSCs) are well-known for their competitive power conversion efficiency (PCE)[1–3] and low production cost.[4–6] Usually, PSCs are fabricated using a metal film as the top electrode. Due to the corrosive nature of the organic–inorganic hybrid perovskite (PVSK hereafter) material, the stability problem is always faced, which hinders the potential application of PSCs in the future.[7,8] Carbon electrodes have long been used as electric-connecting components in dry cells and lithium batteries,[9] and they could bear heavy electrochemical corrosion. As such, it would be appealing to replace the metal electrode by the carbon electrode in PSCs. Owing to the pioneering works done by Han *et al.*, carbon electrode-based PSCs (or CPSCs) have been constructed and several kinds of structures have been proposed, for example, mesoscopic CPSCs (meso CPSCs for short),[4] embedment CPSCs,[10] planar CPSCs,[11] and quasi-planar CPSCs.[12] These CPSCs have shown not only prolonged stability[5,13,14] but also high efficiencies.[10,15–17] Specifically, photo-stability of 1000 h, an outdoor-working-stability of 1 month, and storage stability of over 1 year were achieved in the meso CPSC modules, even without encapsulation.[13] With bulk engineering of the perovskite crystallite [using 4-(aminomethyl) benzoic acid hydroiodide], an efficiency of 15.6% (AM 1.5 G, 100 mW/cm^2) was obtained in the meso CPSCs.[16] Meanwhile, an efficiency of 14.77% and storage stability of 5 months (no encapsulation) were gained in planar CPSCs.[11] Very recently, 16.51% and 15.28% were achieved for meso CPSCs and planar CPSCs, respectively.[18,19] The prolonged stability is due to two facts: one is the inert nature of carbon electrodes and the other is the barrier provided by them. Such carbon electrodes usually come with thickness up to 10 μm or more, which retards the penetration of the H_2O/O_2 from air.[6]

Amongst these device structures, meso CPSCs are known by the advantage of low-cost fabrication. They could be prepared in open air, thus excluding the usage of a nitrogen gas glove. This is appealing to reduce the levelized cost of electricity (LCOE).[20,21] However, the meso CPSCs were usually prepared in high-temperature processes (400–450 °C). To further reduce the production cost, it is essential to lower the fabrication temperature, like that done in metal electrode-based PSCs.[22,23] Here in this article, one such strategy is developed. With the assistance of low-temperature mesoscopic skeleton and vacuum-assisted perovskite formation technique, power conversion efficiency (PCE) > 12% and storage stability >220 days have been obtained.

Low-temperature fabrication procedures of the carbon electrode-based hole-conductor-free and mesoscopic perovskite solar cells (or low-temperature meso CPSCs) are mimicked in Figs. S1(a)–S1(f) in the supplementary material, as well as the related experimental details. Briefly, after the mesoporous skeleton was constructed, a perovskite precursor was added on top and then heated at 50 °C for 0.5 h in a vacuum chamber [Fig. 1(a)], with pressure of about $\sim 1 \times 10^4$ Pa. Then, low-temperature meso CPSCs [Fig. 1(b)] were prepared and ready for performance evaluation. The skeleton of "ITO/SnO_2/mp-TiO_2/mp-ZrO_2/carbon" was adopted and prepared at low temperatures (≤150 °C). For example, the carbon electrode (~20 μm) was prepared using TiO_2 nanoparticles (TiO_2NPs) as binding agents like that documented before.[24] mp-TiO_2 and mp-ZrO_2 layers were made from TiO_2 and ZrO_2 nanocrystallites, respectively. The nanocrystallites are well-crystallized as reflected by Fig. S2 in the supplementary material. Bilayer SnO_2 films were prepared like that described before, with the first/second layers prepared from SnO_2 quantum dots[25] and $SnCl_2$ solution,[26,27] respectively.

The crystallographic properties of the perovskite were studied by x-ray diffraction (XRD). The whole device was irradiated from the top of the devices. As shown in Fig. 1(c), peaks could be observed at around 14.22°, 20.11°, 23.66°, 28.32°, 31.98°, 40.57°, and 43.31°, which correspond to the (110), (112), (111), (004), (310), (202), and (212) planes of $(5\text{-AVA})_x$ $(MA)_{1-x}PbI_3$, respectively.[28] Thus, PVSK crystallites could be crystallized in the low-temperature processed mesoporous skeleton. It is noted that the peak at 26.62° is due to the (110) plane of graphite. In addition, no obvious peaks could be observed for PbI_2.

Cross-sectional morphological properties of the devices were studied by scanning electron microscopy (SEM). The typical results are shown in Fig. 2. It could be seen that for device treated in air, plates

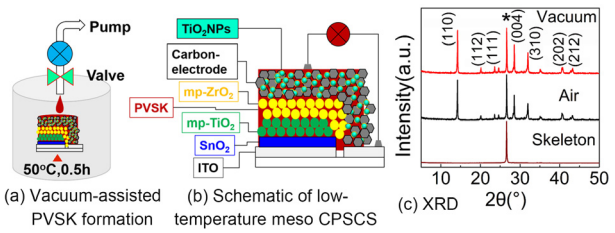

FIG. 1. (a) Schematic of the vacuum-assisted formation process of perovskite crystallites. (b) Device structure of low-temperature meso CPSCs. (c) X-ray diffraction patterns of bare skeleton and full devices with perovskite crystallites formed in air or vacuum.

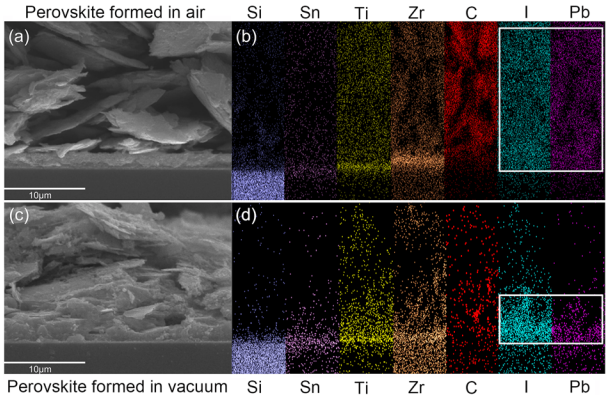

FIG. 2. Typical cross-sectional scanning electron microscope (SEM) images and the corresponding element distribution maps of the low-temperature processed meso CPSCs with the perovskite formed: (a) and (b) in air and (c) and (d) in vacuum. White rectangles represent the distribution regions of perovskite crystallites.

stack loosely, and for that treated in vacuum [Fig. 2(c)], the stack is condensed. These plates are suggested to be graphite according to the experiment. As such, vacuum treatment has modified the structure of the mesoporous skeleton, making it more condensed. On the other hand, the formation behavior of the perovskite crystallites has also been modified. From element distribution maps (EDS) [Figs. 2(b) and 2(d)], one could see that elements of Pb and I distribute uniformly over the whole skeleton (marked by the white rectangle) for devices treated in air. However, for that done in vacuum, Pb and I mainly distribute in the bottom part of the skeleton or the region including mp-TiO_2, mp-ZrO_2, and the bottom part of the carbon electrode. In fact, this region is the core part of the meso CPSCs, whereas photogenerated electron–hole pairs are generated, separated, and collected. Such condensed distribution is helpful for the power conversion processes, as will be revealed later.

The effect of vacuum treatment on film conductance of the carbon electrode was examined. A group of carbon films were prepared on bare glasses and heated at 150 °C in air for 5 h [denoted by "Air" in Fig. 3(a)]; after the film thickness (d) and sheet resistance (R_{sh}) were measured (details referred to the supplementary material), they were further heated at 50 °C in vacuum for 1 h [denoted by "Air + Vacuum" in Fig. 3(a)], after which the film thickness and sheet resistance were measured again. It was observed that when carbon films were treated in air, the film thickness was about 71.6 μm and the sheet resistance (R_{sh}) was about 10.5 ohm/sq, and after the carbon films were further treated in vacuum, they decreased to 65.8 μm and 9.3 ohm/sq, respectively. Accordingly, the average conductivity increased from 13.3 S/cm to 16.4 S/cm. As a result, vacuum treatment has condensed the mesoporous carbon electrode and improved the film conductivity.

Charge-extraction dynamics of the meso CPSCs were studied by the transient photocurrent (TPC) decay curve measurement. As shown in Figs. 3(b) and 3(c), exponential decaying behavior was observed. Charge-extraction time (t_d) was picked by fitting the curves by the exponential function. It is found that for devices treated in air, t_d is 2.76 (±0.61) μs, while for those treated in vacuum, it decreases to 1.94 (±0.52) μs. Thus, the extraction process has been accelerated.

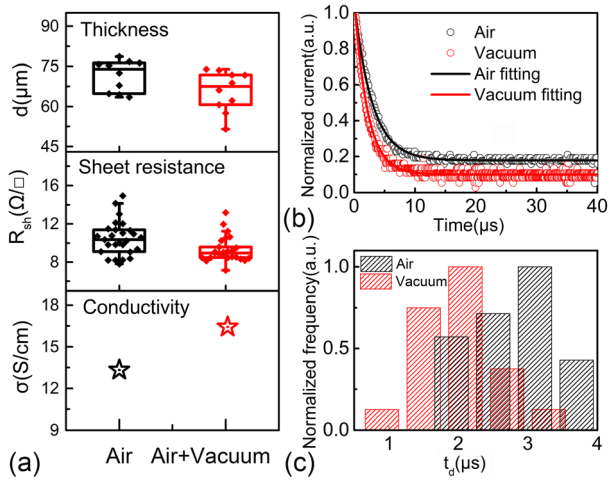

FIG. 3. (a) Effect of vacuum treatment on the film thickness and conductivity of the TiO_2NPs-binding carbon electrode. ("Air" denotes "heating at 150 °C in air for 5 h," while "Air+Vacuum" denotes "heating at 50 °C in vacuum for 1 h" after the air treatment.) (b) Typical transient photocurrent (TPC) decay curves of the low-temperature meso CPSCs with PVSK crystallites formed in air or vacuum. (c) Charge-extraction time picked from the TPC decay curves.

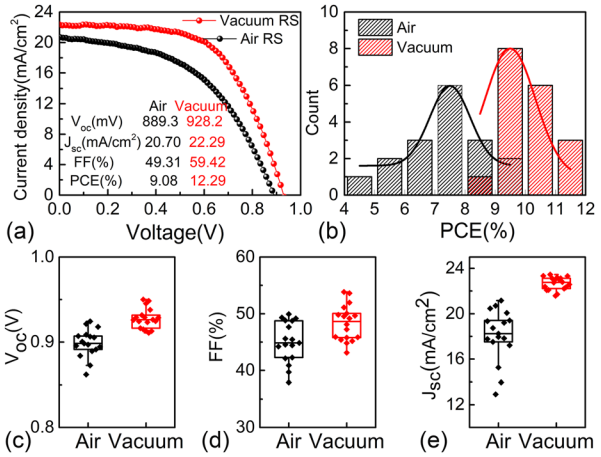

FIG. 4. (a) Typical current-density voltage (*JV*) curves of the low-temperature meso CPSCs (under simulated illumination with the spectrum standard of AM 1.5 G, 100 mW/cm^2, the test area is 0.0514 cm^2, recorded by reverse scan, marked by RS). Statistics on performance parameters (reverse scan) of (b) *PCE*, (c) V_{OC}, (d) *FF*, and (e) J_{SC}.

The improvement is ascribed to two facts: one is the concentrated distribution of PVSK crystallites and the other is the strengthened contact between PVSK crystallites and charge-extraction layers (mp-TiO_2 and the carbon electrode). Due to the above two reasons, the photo-generated charges could be extracted more quickly.

Photo-to-electric power conversion properties of the low-temperature meso CPSCs were studied by recording the current density–voltage (*JV*) curves under simulated illumination (AM 1.5 G, 100 mW/cm^2). Typical *JV* curves and performance parameters are presented in Fig. 4. It could be found that vacuum treatment has improved all of the four performance parameters, like open-circuit voltage (V_{OC}), short-circuit current density (J_{SC}), fill factor (*FF*), and power conversion efficiency (*PCE*). Concretely, V_{OC} increases from 898.6(±16.3) mV to 927.4 (±11.9) mV, J_{SC} increases from 18.10 (±2.29) mA/cm^2 to 22.67 (±0.58) mA/cm^2, *FF* rises from 45.04 (±3.61)% to 48.34 (±3.12)%, and *PCE* upgrades from 7.38 (±1.40)% to 10.17 (±0.86)%. The optimized device performance reaches 12.29%. Such performance is comparable to the previously reported high-temperature meso CPSCs[28–30] and also to the device assembled from high-temperature mp-TiO_2/mp-ZrO_2 and low-temperature carbon electrodes.[31]

The improved performance could be understood from four aspects. The first is the vacuum-assisted perovskite formation. As stated above, PVSK crystallites could be concentrated to the core part of the mesoporous skeleton (mp-TiO_2/mp-ZrO_2/bottom of the carbon electrode). This could accelerate the extraction, while retarding the recombination of the photo-generated charge-carriers. The second is the improved conductivity of the TiO_2NPs-binding carbon electrode, which is also helpful in elevating the *FF*. The third one is the low-temperature compatible SnO_2 layer. As shown by You, Fang, and co-workers, [23,32–34] the SnO_2 thin film processed at low temperature could serve as an excellent electron-extraction layer due to the good conductivity and favorable energy level. Finally, like that done in low-temperature dye-sensitized solar cells, the mp-TiO_2 film produced from well-crystallized TiO_2 nanocrystallites could serve as an efficient electron-extraction material too.[35,36] From the PCE distribution [Fig. 4(b)], one can also find that a higher yield is obtained for devices using vacuum-assisted perovskite formation. In addition, less hysteresis was also observed for devices treated in vacuum (Fig. S3 and Table S1). As a consequence, such a low-temperature strategy is reproducible. Honestly, the device efficiency obtained currently is relatively lower than other kinds of PSCs. The main problem lies on the relatively low V_{OC} and *FF*. Both of these relate closely to the charge transfer and recombination processes. First, the formation process of the perovskite crystallites is confined by the mesoporous structure. Thus, relative heavier recombination might be involved due to small perovskite crystallites formed in the mesoporous skeleton. Second, the hole-extraction ability of the carbon electrode should be further improved. Compared with the star hole-conductor, for example, the spiro-OMeTAD (with the valence-band maximum of about −5.22 eV[37]), the work function of the carbon electrode is relatively low. To further upgrade the device efficiency, it is essential to reduce the charge recombination and accelerate the charge extraction processes.

The storage stability of the low temperature meso CPSCs was tested by storing the devices in the dark (with a relative humidity of 40%–60%, without encapsulation). As shown in Fig. 5, for devices treated in air, the efficiency decreases from the initial one of ∼6% to that of ∼2% after about 2 months. However, for those treated in vacuum, the efficiency remained nearly unchanged for more than 7 months (225 days). Similar behavior was observed in all of the other three performance parameters or J_{SC}, V_{OC}, and *FF*. Such an improvement is due to the modification to the mesoporous skeleton, which has been brought by the vacuum treatment.

The improved stability is ascribed to two key parameters: one is the vacuum treatment and the other is the TiO_2NPs. Vacuum treatment has condensed the porous skeleton and concentrated perovskite distribution. As shown in Fig. 6(a), when it is pumped, negative

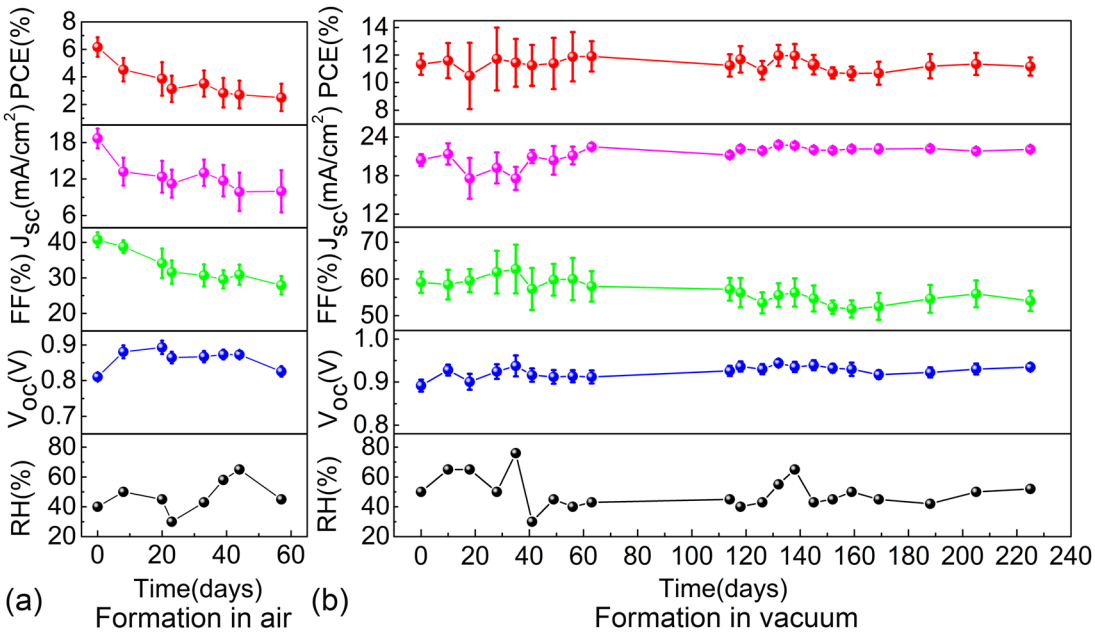

FIG. 5. Storage stability of the low-temperature meso CPSCs with PVSK crystallites formed: (a) in air and (b) in vacuum (no encapsulation was used, and the relative humidity was 40%–60%).

pressure appears between the skeleton and the vacuum chamber. Thus, the residential gas could move to the outside of the skeleton [Fig. 6(b)], which in return helps the penetration of the perovskite precursor into the deeper part of the skeleton. Meanwhile, the dehydration reaction could take place in the carbon electrode [Fig. 6(d)]. As documented before, there exist much surface hydroxyl groups (-OH) on both TiO_2NPs and carbon particles.[24,38] When it is heated in vacuum, H_2O molecules are easier to escape. As such, the dehydration process is accelerated, which condenses the mesoporous carbon electrode [Fig. 6(c)], which prevents the moisture to penetrate and prolongs the device stability. In fact, the condensing behavior was also revealed during the early trivial of the study. We treated the mesoporous skeleton in vacuum but happened to find that the obtained skeleton could hardly be penetrated by the precursor, as shown by the photoimage in Fig. S4(b).

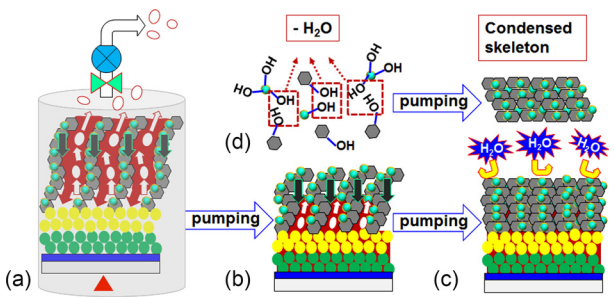

FIG. 6. Schematics showing the effect vacuum treatment on the construction of low-temperature meso CPSCs. (a) Schematic of the vacuum treatment, (b) infiltration process of the perovskite precursor, (c) resultant device with the condensed skeleton and compactly distributed perovskite crystallites, and (d) schematic figure of the dehydration process.

Finally, efficient and stable hole-conductor-free, mesoscopic perovskite solar cells based on the carbon electrode (meso CPSCs) have been fabricated by low-temperature procedures. With the assistance of the vacuum-assisted perovskite formation technique and the low-temperature mesoporous skeleton, power conversion efficiency > 12% and storage stability > 220 days have been achieved, which are helpful to further reduce the production cost.

See the supplementary material for the device preparation and characterization, diagram of fabrication of the mesoporous skeleton for the low-temperature meso CPSCs (Fig. S1), x-ray diffraction patterns of TiO_2 and ZrO_2 powders used in current work (Fig. S2), comparison between current density–voltage curves of low-temperature meso CPSCs (Fig. S3), effect of vacuum treatment on the mesoporous skeleton (Fig. S4), and hysteresis indexes of the low-temperature meso CPSCs (Table S1).

T. Shi and S. Lin acknowledge the support from the Fundamental Research Funds for the Central South University (Nos. 2020zzts365 and 2020zzts045, respectively). C. Zhou acknowledges support from the Natural Science Foundation of China (NSFC, No. 61774170) and the Natural Science Foundation of Hunan Province (No. 2020JJ4759). Y. Gao acknowledges support from the National Science Foundation, United States (NSF, Nos. CBET-1437656 and DMR-1903962). Y. Yuan acknowledges support from the Natural Science Foundation of China (NSFC, No. 51673218). Y. Yuan and C. Zhou acknowledge support from the Innovation-Driven Project of Central South University (No. 2020CX006).

DATA AVAILABILITY

The data that support the findings of this study are available within the article and its supplementary material.

REFERENCES

[1]NREL PV Research Cell Record Efficiency Chart, see https://www.nrel.gov/pv/cell-efficiency.html (last accessed June 2020).
[2]E. H. Jung, N. J. Jeon, E. Y. Park, C. S. Moon, T. J. Shin, T. Y. Yang, J. H. Noh, and J. Seo, Nature **567**(7749), 511–515 (2019).
[3]N. J. Jeon, H. Na, E. H. Jung, T.-Y. Yang, Y. G. Lee, G. Kim, H.-W. Shin, S. I. Seok, J. Lee, and J. Seo, Nat. Energy **3**(8), 682–689 (2018).
[4]Z. Ku, Y. Rong, M. Xu, T. Liu, and H. Han, Sci. Rep. **3**, 3132 (2013).
[5]A. Mei, X. Li, L. Liu, Z. Ku, T. Liu, Y. Rong, M. Xu, M. Hu, J. Chen, Y. Yang, M. Grätzel, and H. Han, Science **345**(6194), 295–298 (2014).
[6]C. Zhou and S. Lin, Sol. RRL **4**(2), 1900190 (2020).
[7]Y. Kato, L. K. Ono, M. V. Lee, S. Wang, S. R. Raga, and Y. Qi, Adv. Mater. Interfaces **2**(13), 1500195 (2015).
[8]D. Wei, T. Wang, J. Ji, M. Li, P. Cui, Y. Li, G. Li, J. M. Mbengue, and D. Song, J. Mater. Chem. A **4**(5), 1991–1998 (2016).
[9]M. Xia, Y. Li, Y. Wu, H. Zhang, J. Yang, N. Zhou, Z. Zhou, and X. Xiong, Appl. Surf. Sci. **480**, 410–418 (2019).
[10]Z. Wei, H. Chen, K. Yan, and S. Yang, Angew. Chem., Int. Ed. **53**(48), 13239–13243 (2014).
[11]J. Yan, S. Lin, X. Qiu, H. Chen, K. Li, Y. Yuan, M. Long, B. Yang, Y. Gao, and C. Zhou, Appl. Phys. Lett. **114**(10), 103503 (2019).
[12]Z. Yu, B. Chen, P. Liu, C. Wang, C. Bu, N. Cheng, S. Bai, Y. Yan, and X. Zhao, Adv. Funct. Mater. **26**(27), 4866–4873 (2016).
[13]Y. Hu, S. Si, A. Mei, Y. Rong, H. Liu, X. Li, and H. Han, Sol. RRL **1**(2), 1600019 (2017).
[14]Y. Rong, Y. Hu, A. Mei, H. Tan, M. I. Saidaminov, S. I. Seok, M. D. McGehee, E. H. Sargent, and H. Han, Science **361**(6408), eaat8235 (2018).
[15]Y. Rong, X. Hou, Y. Hu, A. Mei, L. Liu, P. Wang, and H. Han, Nat. Commun. **8**, 14555 (2017).
[16]Y. Hu, Z. Zhang, A. Mei, Y. Jiang, X. Hou, Q. Wang, K. Du, Y. Rong, Y. Zhou, G. Xu, and H. Han, Adv. Mater. **30**(11), 1705786 (2018).
[17]Y. Yang, Z. Liu, W. K. Ng, L. Zhang, H. Zhang, X. Meng, Y. Bai, S. Xiao, T. Zhang, C. Hu, K. S. Wong, and S. Yang, Adv. Funct. Mater. **29**(1), 1806506 (2019).
[18]Z. Liang, B. Yang, A. Mei, S. Lin, H. Han, Y. Yuan, H. Xie, Y. Gao, and C. Zhou, Chin. Phys. B **29**(7), 078401 (2020).
[19]Y. Sheng, W. Ji, Y. Chu, Y. Ming, A. Mei, Y. Hu, Y. Rong, and H. Han, Sol. RRL **4**, 2000185 (2020).
[20]Z. Li, Y. Zhao, X. Wang, Y. Sun, Z. Zhao, Y. Li, H. Zhou, and Q. Chen, Joule **2**(8), 1559–1572 (2018).
[21]M. Cai, Y. Wu, H. Chen, X. Yang, Y. Qiang, and L. Han, Adv. Sci. **4**(1), 1600269 (2017).
[22]Y. Deng, X. Zheng, Y. Bai, Q. Wang, J. Zhao, and J. Huang, Nat. Energy **3**(7), 560–566 (2018).
[23]H. Liu, Z. Chen, H. Wang, F. Ye, J. Ma, X. Zheng, P. Gui, L. Xiong, J. Wen, and G. Fang, J. Mater. Chem. A **7**(17), 10636–10643 (2019).
[24]L. Xu, F. Wan, Y. Rong, H. Chen, S. He, X. Xu, G. Liu, H. Han, Y. Yuan, J. Yang, Y. Gao, B. Yang, and C. Zhou, Org. Electron. **45**, 131–138 (2017).
[25]G. Yang, C. Chen, F. Yao, Z. Chen, Q. Zhang, X. Zheng, J. Ma, H. Lei, P. Qin, L. Xiong, W. Ke, G. Li, Y. Yan, and G. Fang, Adv. Mater. **30**(14), 1706023 (2018).
[26]X. Qiu, B. Yang, H. Chen, G. Liu, Y. Liu, Y. Yuan, H. Huang, H. Xie, D. Niu, Y. Gao, and C. Zhou, Org. Electron. **58**, 126–132 (2018).
[27]F. Wan, X. Qiu, H. Chen, Y. Liu, H. Xie, J. Shi, H. Huang, Y. Yuan, Y. Gao, and C. Zhou, Org. Electron. **59**, 184–189 (2018).
[28]H. Chen, K. Li, H. Liu, Y. Gao, Y. Yuan, B. Yang, and C. Zhou, Org. Electron. **61**, 119–124 (2018).
[29]K. Li, H. Chen, H. Liu, Y. Yuan, Y. Gao, B. Yang, and C. Zhou, Org. Electron. **62**, 298–303 (2018).
[30]H. Liu, B. Yang, H. Chen, K. Li, G. Liu, Y. Yuan, Y. Gao, and C. Zhou, Org. Electron. **58**, 69–74 (2018).
[31]S. Wang, P. Jiang, W. Shen, A. Mei, S. Xiong, X. Jiang, Y. Rong, Y. Tang, Y. Hu, and H. Han, Chem. Commun. **55**(19), 2765–2768 (2019).
[32]Q. Jiang, X. Zhang, and J. You, Small **14**(31), 1801154 (2018).
[33]Q. Jiang, Y. Zhao, X. Zhang, X. Yang, Y. Chen, Z. Chu, Q. Ye, X. Li, Z. Yin, and J. You, Nat. Photonics **13**(7), 460–466 (2019).
[34]J. Ma, X. Zheng, H. Lei, W. Ke, C. Chen, Z. Chen, G. Yang, and G. Fang, Sol. RRL **1**(10), 1700118 (2017).
[35]P. Zhang, C. Wu, Y. Han, T. Jin, B. Chi, J. Pu, and L. Jian, J. Am. Ceram. Soc. **95**(4), 1372–1377 (2012).
[36]T. Miyasaka, M. Ikegami, and Y. Kijitori, J. Electrochem. Soc. **154**(5), A455–A461 (2007).
[37]N. J. Jeon, H. G. Lee, Y. C. Kim, J. Seo, J. H. Noh, J. Lee, and S. I. Seok, J. Am. Chem. Soc. **136**(22), 7837–7840 (2014).
[38]C. Zhou, X. Zhao, B. Yang, D. Zhang, Z. Li, and K. Zhou, J. Colloid Interface Sci. **374**, 9–17 (2012).